# Elementary excitations of a system of one-dimensional chiral fermions with short-range interactions

K. A. Matveev

Materials Science Division, Argonne National Laboratory, Argonne, Illinois 60439, USA (Dated: February 3, 2023)

We study general features of the excitation spectrum of a system of one-dimensional chiral spinless fermions with short-range interactions. We show that the nature of the elementary excitations of such a system depends strongly on the nonlinearity of the underlying dispersion of the fermions. In the case of quadratic nonlinearity, the low-momentum excitations are essentially fermionic quasiparticles and quasiholes, whereas the high-momentum ones are classical harmonic waves and solitons. In the case of cubic nonlinearity, the nature of the elementary excitations does not depend on momentum and is determined by the strength of the interactions. At a certain critical value of the interaction strength the excitation spectrum changes qualitatively, pointing to a dynamic phase transition in the system.

#### I. INTRODUCTION

The effect of interactions on the low-energy properties of systems of fermions is strongly enhanced in one dimension. Indeed, in three dimensions such a system can be described by the Fermi liquid theory [1], in which the elementary excitations are similar to those of the Fermi gas. On the other hand, the low-energy properties of systems of interacting one-dimensional fermions are commonly described in the framework of the Luttinger liquid theory [2, 3], in which excitations have bosonic statistics. The best known signature of the Luttinger liquid behavior is the power-law renormalization of the tunneling density of states [4, 5].

The issue of the nature of the elementary excitations of the Luttinger liquid is rather subtle. At low energies many properties of the system, including the tunneling density of states, are described by the Luttinger model, in which the dispersion of the fermions is approximated by two linear chiral branches [6]. In the absence of interactions, the many-body spectrum of this model is highly degenerate. The Hamiltonian of the system can be presented as that of the system of the original fermions or as that of noninteracting bosons. Importantly, the degeneracy is lifted when nontrivial interactions of the fermions are included in the Luttinger model. Typical interactions destroy the picture of free fermionic quasiparticles, whereas the bosons remain noninteracting, albeit with a nonlinear dispersion. Alternatively, the degeneracy of the spectrum can be lifted by including nonlinear corrections to the dispersion of the fermions. This perturbation preserves the picture of free fermionic quasiparticles, but generates interactions of bosonic excitations.

In a typical physical realization of one-dimensional fermions, the dispersion is nonlinear and interactions are not negligible. The nonlinearity is usually quadratic,  $\delta\epsilon_p^{(f)}=p^2/2m$ , where m is the effective mass of the particles at the Fermi level. On the other hand, for the short-range interactions, the nonlinearity of the bosonic spectrum is cubic,  $\delta\epsilon_p^{(b)}=\zeta p^3$ . At low energies, corresponding to  $p\ll p^*\sim (m\zeta)^{-1}$ , the nonlinearity of the

fermion dispersion is the dominant perturbation to the Luttinger model at low energies, and the elementary excitations are fermions [7].

The elementary excitations of a system of onedimensional fermions can be studied in detail [8, 9] in the case of strong repulsive interactions, where the crossover momentum  $p^*$  is small compared to the Fermi momentum  $p_F$ . At low energies the Hamiltonian of the system splits into two chiral Hamiltonians, which can be reduced [9] to the quantum Korteweg-de Vries (KdV) model [10, 11]. At  $p \ll p^*$  the system has two branches of elementary excitations near each Fermi point, with dispersions showing quadratic nonlinearities,  $\delta \varepsilon_p = \pm p^2/2m^*$ . They correspond to the fermionic quasiparticle and quasihole expected from Ref. [7]. The dispersion undergoes a crossover at  $p \sim p^*$ . At  $p \gg p^*$  the quantum KdV Hamiltonian approaches the classical limit. In this regime one of the excitation branches becomes a boson and has a nonlinear dispersion with  $\delta \varepsilon_p \propto p^3$ , as expected from the Luttinger model with short-range interactions. The second branch corresponds to the classical KdV soliton; the nonlinearity of its dispersion is  $\delta \varepsilon_p \propto p^{5/3}$ .

The goal of this paper is to study the spectrum of the elementary excitations of a system of interacting chiral spinless fermions, such as those at the edge of the integer Quantum Hall system [12] with occupation fraction  $\nu = 1$ . We will limit ourselves to the case of shortrange interaction and assume that the dispersion of the fermions has either quadratic or cubic nonlinearity. The case of quadratic nonlinearity is relatively straightforward, because upon bosonization [2] the Hamiltonian of the system again reduces to that of the quantum KdV model [10, 11]. The case of cubic nonlinearity of the fermion dispersion,  $\delta \epsilon_p^{(f)} = \gamma p^3$ , is qualitatively different. Most importantly, because the dispersion of the bosonic excitations of the Luttinger liquid also has cubic nonlinearity,  $\delta \epsilon_p^{(b)} = \zeta p^3$ , the relative significance of the dispersion curvature and interactions does not depend on momentum. The crossover between the regimes of fermionic and bosonic excitations is controlled by the effective interaction strength  $\zeta/\gamma$ . Upon bosonization,

the Hamiltonian of the system reduces to that of the quantum modified KdV (mKdV) model [11]. Although the latter is known to be integrable [10], no exact results for the dispersion of the elementary excitations are available. We study the excitation spectrum of this model numerically and identify the limits where the elementary excitations are either fermionic quasiparticles and quasiholes, or semiclassical phonons and solitons.

The paper is organized as follows. In Sec. II we study the case of chiral fermions with quadratic dispersion. In particular, we demonstrate that the boundaries of the many-body spectrum coincide with the two branches of the elementary excitations of the system. In Sec. III we study the case of cubic dispersion. We compute the boundaries of its many-body spectrum numerically and identify the regions where they correspond to the elementary excitations of the system. We summarize and discuss our results in Sec. IV.

### II. CHIRAL FERMIONS WITH QUADRATIC DISPERSION

We consider systems of spinless chiral one-dimensional fermions with two-body interactions. In general, the Hamiltonian of such a system has the form

$$\hat{H} = \sum_{p} \epsilon_{p} : c_{p}^{\dagger} c_{p} : + \frac{1}{L} \sum_{\substack{p_{1}p_{2} \\ q>0}} V(q) c_{p_{1}+q}^{\dagger} c_{p_{1}} c_{p_{2}}^{\dagger} c_{p_{2}+q}.$$
 (1)

Here the operator  $c_p$  annihilates a fermion in a state with momentum p and energy  $\epsilon_p$ , and L is the system size. We assume periodic boundary conditions, and thus p and q are integer multiples of  $2\pi\hbar/L$ . The notation  $:\dots:$  indicates normal ordering of the fermion operators with respect to the ground state  $|0\rangle$ , in which all the fermionic states with  $p \leq 0$  are filled and those with p > 0 are empty.

We are interested in the case of short-range interactions, for which the Fourier transform of the interaction potential V(q) is well defined at q=0 along with its second derivative [13]. At sufficiently small q we then approximate

$$V(q) = V(0) - \eta q^2, (2)$$

where  $\eta = -V''(0)/2$ . For typical repulsive interactions V(0) and  $\eta$  are positive.

A single-channel system of chiral fermions has only one Fermi point  $p_F$ . As discussed above, even in the vicinity of the Fermi level it is important to account for the nonlinearity of the dispersion  $\epsilon_p$ . In this Section, we consider the generic case, in which the nonlinearity of the dispersion near  $p_F$  is quadratic,

$$\epsilon_p = v_F(p - p_F) + \frac{(p - p_F)^2}{2m}.$$
(3)

Here  $v_F$  and m are the Fermi velocity and the effective mass. To simplify the treatment of the finite-size effects

we define  $p_F = \pi \hbar/L$ , which is equidistant from the highest occupied single particle state p=0 and the lowest unoccupied state  $p=2\pi \hbar/L$  in the many-body ground state  $|0\rangle$ .

To make further progress we bosonize the Hamiltonian given by Eqs. (1)–(3) using the standard expression [2] for the fermion annihilation operator at point x,

$$\Psi(x) = \frac{1}{\sqrt{L}}U : e^{i\phi(x)} : . \tag{4}$$

The field  $\phi(x)$  is expressed in terms of the bosonic annihilation operators  $b_l$  as

$$\phi(x) = 2\pi N \frac{x}{L} - \sum_{l=1}^{\infty} \frac{i}{\sqrt{l}} \left( e^{i2\pi lx/L} b_l - e^{-i2\pi lx/L} b_l^{\dagger} \right). \tag{5}$$

Here N is the operator of the number of particles measured from that in the ground state  $|0\rangle$ ; the operator U lowers the number of particles by 1, i.e., [U,N]=U. The colons in Eq. (4) denote the normal ordering of the bosonic operators  $b_l$  and  $b_l^{\dagger}$ .

Expressing the fermion operators  $c_p$  in the Hamiltonian (1) in terms of the bosonic field  $\phi(x)$  with the help of Eq. (4) and substituting Eqs. (2) and (3), we obtain

$$\hat{H} = v(\hat{P} - p_F N) - \frac{\pi^2 \hbar^2 N}{6mL^2} + \hat{H}_{KdV}.$$
 (6)

Here  $v = v_F + V(0)/2\pi\hbar$ , and  $\hat{P}$  is the operator of the total momentum of the system,

$$\hat{P} = p_F N + \frac{\hbar}{4\pi} \int_{-L/2}^{L/2} : (\partial_x \phi)^2 : dx$$

$$= \frac{\pi \hbar N (N+1)}{L} + \sum_{l=1}^{\infty} \frac{2\pi \hbar l}{L} b_l^{\dagger} b_l, \tag{7}$$

measured from that of the ground state  $|0\rangle$ . The last term in Eq. (6) is given by

$$\hat{H}_{KdV} = \frac{\hbar^2}{12\pi m} \int_{-L/2}^{L/2} : [(\partial_x \phi)^3 - a^* (\partial_x^2 \phi)^2] : dx, \quad a^* = \frac{3m\eta}{2\pi}.$$
(8)

Equations (6)–(8) fully account for the effects of changing particle number in the system. In the following, we limit ourselves to the sector of the Hilbert space corresponding to a fixed number of particles. In this case, without loss of generality one can set N=0, resulting in

$$\hat{H} = v\hat{P} + \hat{H}_{KdV}. \tag{9}$$

Since the Hamiltonian (1) conserves momentum, we conclude that  $\hat{H}$  and  $\hat{H}_{\text{KdV}}$  have common eigenstates and that the corresponding energies of any state with momentum p are related by

$$\varepsilon(p) = vp + \varepsilon_{KdV}(p),$$
 (10)

where  $\varepsilon$  and  $\varepsilon_{\text{KdV}}$  are the eigenvalues of the Hamiltonians  $\hat{H}$  and  $\hat{H}_{\text{KdV}}$ , respectively.

In combination with the commutation relation

$$[\phi(x), \partial_y \phi(y)] = -2\pi i \delta(x - y), \tag{11}$$

which follows from Eq. (5), the Hamiltonian (8) defines the quantum KdV problem [10]. It can also be obtained [9] by applying a certain limiting procedure to the bosonized Hamiltonian of either the Lieb-Liniger model [14], or the hyperbolic Calogero-Sutherland model [15, 16]. The latter two models have Bethe ansatz solutions, and their elementary excitations are well understood. Using those results, the exact dispersions of the elementary excitations of the quantum KdV model at  $L \to \infty$  have been obtained in Ref. [9],

$$\varepsilon_{\rm KdV}(p) = \frac{p^{*2}}{2m} e_{\pm} \left(\frac{p}{p^{*}}\right).$$
 (12)

Here  $p^* = 3\hbar/2a^*$ , which in our notations takes the form

$$p^* = \frac{\pi\hbar}{m\eta}. (13)$$

The dimensionless functions  $e_{+}(s)$  and  $e_{-}(s)$  correspond to the two branches of the elementary excitations. Their exact analytic expressions (in quadratures) can be found in Ref. [9]; here we quote their limiting behaviors at large and small s. For the upper branch we have

$$e_{+}(s) = \begin{cases} s^{2}, & s \ll 1\\ \frac{3}{5} \left(\frac{2\pi}{3}\right)^{2/3} s^{5/3}, & s \gg 1, \end{cases}$$
 (14)

whereas for the lower one,

$$e_{-}(s) = \begin{cases} -s^2, & s \ll 1\\ -s^3, & s \gg 1. \end{cases}$$
 (15)

The dispersions of the elementary excitations are illustrated in Fig. 1.

The above asymptotic expressions for the energies of the elementary excitations allow for simple physical interpretations. The scaling dimensions of the first and second terms in the Hamiltonian density in Eq. (8) are 3 and 4, respectively. Thus at small momentum the second term, which accounts for the interactions of fermions, can be neglected. The remaining term accounts for the quadratic nonlinearity of the dispersion of the fermions. Indeed, at  $p \ll p^*$ , Eqs. (12), (14), and (15) yield quasiparticle dispersions  $\varepsilon_{\rm KdV} = \pm p^2/2m$ , which correspond to the fermionic quasiparticle and quasihole excitations.

At large momentum  $p \gg p^*$ , the system is in the interaction dominated regime. Substituting Eq. (5) into the second term in Eq. (8), we bring the interaction Hamiltonian to the form

$$H_{\rm int} = -\frac{\eta}{2\pi\hbar} \sum_{l=1}^{\infty} p_l^3 b_l^{\dagger} b_l, \quad p_l = \frac{2\pi\hbar}{L} l.$$
 (16)

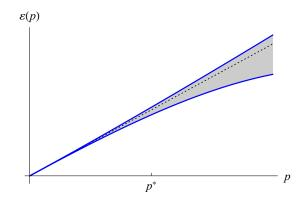


FIG. 1. Dispersions of the two branches of the elementary excitations of the system of interacting chiral fermions with quadratic dispersion. The two solid lines are obtained by combining Eqs. (10) and (12), with the (arbitrarily chosen) velocity value  $v = 10p^*/m$ . The dotted line shows the linear part of the dispersion relation,  $\varepsilon(p) = vp$ . All the eigenstates of the system are confined to the shaded region between the solid lines.

Thus at large momentum  $p \gg p^*$ , the nonlinear correction to the energy of the bosonic excitations in the Luttinger liquid approximation scales as  $-p^3$ , in agreement with the second line of Eq. (15). To obtain the physical interpretation of the other mode, one should restore the small first term in Eq. (8) and derive the equation of motion for the particle density operator  $\partial_x \phi/2\pi$ . At  $p \gg p^*$  and  $L \to \infty$ , it becomes the classical KdV equation [9]. The latter has two types of solutions. First, there are solutions representing harmonic waves of infinitesimal amplitude, which have cubic dependence of frequency on the wavevector. They are equivalent to the bosonic excitations in Eq. (16). Second, there are soliton solutions of the KdV equation, for which the energy scales as  $p^{5/3}$  [9]. They correspond to the second line of Eq. (14).

Let us now discuss the full many-body energy spectrum of the Hamiltonian (8). In the absence of interactions,  $\eta = 0$ , each of the two simplest many-body states with momentum p contains only a single elementary excitation, quasiparticle or quasihole, and the corresponding energies are  $p^2/2m$  and  $-p^2/2m$ , respectively. Since any state of the system can be viewed as a combination of particles and holes, and all excitations of a chiral system have positive momenta, the quasiparticle energies  $\pm p^2/2m$  are the highest and lowest energies possible at the total momentum p. Because the Bethe ansatz eigenstates at  $\eta \neq 0$  can also be classified by occupation numbers of quasiparticles and quasiholes, it is natural to expect [8] that the two branches of elementary excitations (12) represent exact boundaries of the many-body spectrum at any interaction strength. This argument applies to many-body states with only a few quasiparticles and quasiholes, because their interactions vanish in the limit of infinite system size. A generic state, however, has a finite density of quasiparticles and quasiholes, and the

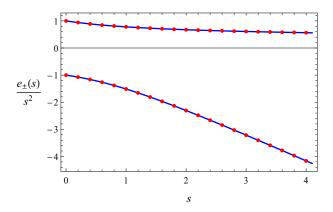


FIG. 2. Comparison of the quasiparticle energies (12) with the spectral boundaries of the Hamiltonian (8). The horizontal axis s is the momentum in units of  $p^*$  given by Eq. (13). The solid lines are the energies (12) divided by  $p^2/2m$ . The dots represent the numerically computed boundaries of the energy spectrum of the Hamiltonian (8) extrapolated to infinite system size.

above simple argument does not apply. Nevertheless, we conjecture that Eq. (12) yields the exact boundaries of the excitation spectrum at any  $\eta$ . For the system of interacting chiral fermions defined by Eqs. (1)–(3), this means that the full energy spectrum is confined to the shaded region in Fig. 1.

We now verify the above conjecture by numerical diagonalization of the quantum KdV Hamiltonian (8). In Fig. 2 we plot the upper and lower boundaries of the spectrum normalized by  $p^2/2m$ . The conjectured values of the boundaries are given by Eq. (12), which upon normalization yields  $e_{\pm}(s)/s^2$ , where  $s=p/p^*$ . We used the analytic expressions for  $e_+(s)$  obtained in Ref. [9] and plotted  $e_{\pm}(s)/s^2$  as solid lines in Fig. 2. The horizontal axis represents  $s = p/p^* = pm\eta/\pi\hbar$ , see Eq. (13). In the numerical calculation, we fix the total momentum p and find the highest and lowest eigenvalues of the Hamiltonian (8) for different values of the interaction strength  $\eta$ . The eigenvalues are then divided by  $p^2/2m$  and the results are extrapolated numerically to the limit of infinite system size [17]. The resulting spectral boundaries are shown by dots in Fig. 2. They are in excellent agreement with the conjectured values.

To summarize the results of this Section, we have studied the elementary excitations of the system of interacting chiral spinless fermions described by Eqs. (1)–(3). Upon bosonization, the Hamiltonian reduces to that of the quantum KdV model, see Eq. (8). At low momentum, the excitations are the fermionic quasiparticle and quasihole. At high momentum they become the KdV soliton and the harmonic wave. The energies are given by Eqs. (10) and (12), where the exact expressions for the functions  $e_{\pm}(s)$  can be found in Ref. [9]. The two quasiparticle branches are shown in Fig. 1. They represent the exact boundaries of the many-body spectrum of the system.

#### III. CHIRAL FERMIONS WITH CUBIC DISPERSION

#### A. Hamiltonian

We now turn to the special regime of the interacting system of spinless chiral fermions, in which the Fermi momentum  $p_F$  coincides with an inflection point of the dispersion  $\epsilon_p$ . In this case the effective mass m is infinite, and  $\epsilon_p$  has a cubic nonlinearity near the Fermi point,

$$\epsilon_p = v_F(p - p_F) + \gamma (p - p_F)^3. \tag{17}$$

In the following, we assume  $\gamma > 0$ . The results for negative  $\gamma$  can be obtained by trivial symmetry transformations.

Next, we apply the bosonization transformation (4) to bring the Hamiltonian given by Eqs. (1), (2), and (17) to the form

$$\hat{H} = \left(v - \frac{\pi^2 \hbar^2 \gamma}{L^2}\right) (\hat{P} - p_F N) + \hat{H}_{\text{mKdV}}.$$
 (18)

Here again  $v = v_F + V(0)/2\pi\hbar$ , the operator of the total momentum is defined by Eq. (7), and we again chose the Fermi momentum  $p_F = \pi\hbar/L$ . The last term is given by

$$H_{\text{mKdV}} = \frac{\hbar^3 \gamma}{8\pi} \int_{-L/2}^{L/2} : [(\partial_x \phi)^4 + (1 - 2\chi)(\partial_x^2 \phi)^2] : dx, \quad (19)$$

where  $\chi = \eta/2\pi\hbar\gamma$ . In combination with the commutation relation (11), the Hamiltonian (19) defines the quantum mKdV problem [10]. In the limit of infinite system size, the relation between the quantum mKdV Hamiltonian and that of chiral fermions was discussed in Ref. [11].

Unlike the case of quadratic nonlinearity (3), the Hamiltonian given by Eqs. (1), (2), and (17) possesses particle-hole symmetry, i.e., it retains its form under the transformation

$$c_{p_F+q} \to c_{p_F-q}^{\dagger}, \quad \Psi(x) \to \Psi^{\dagger}(x)e^{i2\pi x/L}.$$
 (20)

In the bosonized form, this property is expressed as

$$U \to U^{\dagger}, \quad \phi(x) \to -\phi(x), \quad b_l \to -b_l, \quad N \to -N,$$
(21)

see Eqs. (4) and (5).

Since the Hamiltonian  $\hat{H}$  conserves the total momentum  $\hat{P}$ , it follows from Eq. (18) that it has the same eigenstates at  $H_{\rm mKdV}$ . In the sector of the Hilbert space with the number of particles equal to that in the ground state  $|0\rangle$  one should set N=0. In this case, the eigenvalues of the two Hamiltonians are related by

$$\varepsilon(p) = vp + \varepsilon_{\text{mKdV}}(p),$$
 (22)

where we omitted the finite size correction to the velocity v in Eq. (18).

#### B. Boundaries of the energy spectrum

Our next goal is to study the boundaries of the energy spectrum of the quantum mKdV Hamiltonian (19) in the limit of infinite system size,  $L \to \infty$ . We start with the case of free fermions, corresponding to  $\chi=0$ . In this case, the system supports two types of elementary excitations, the quasiparticles and quasiholes. The particle-hole symmetry of the Hamiltonian (19) ensures that the quasiparticles and quasiholes with momentum p have the same energy  $\gamma p^3$ . The latter is the highest energy of any eigenstate of the Hamiltonian (19) with momentum p at  $\chi=0$ . The lowest possible energy at  $L\to\infty$  is 0. To obtain an eigenstate with energy near this lower boundary, the total momentum p should be divided among many particle-hole pairs, each carrying a very small fraction of the total momentum.

In addition to the case of vanishing interactions,  $\chi = 0$ , the Hamiltonian (19) can be easily treated analytically in the limits of strong repulsive or attractive interactions,  $\chi \to \pm \infty$ . In this case, the second term in Eq. (19) dominates. Using Eq. (5), the latter can be written in terms of the bosonic operators  $b_l$ ,

$$H_{\rm mKdV} \simeq \gamma \left(\frac{1}{2} - \chi\right) \sum_{l=1}^{\infty} p_l^3 b_l^{\dagger} b_l, \quad p_l = \frac{2\pi\hbar}{L} l,$$
 (23)

cf. Eq. (16). A system described by the Hamiltonian (23) has bosonic elementary excitations with energies  $\gamma(\frac{1}{2}-\chi)p^3$ . This expression also yields the lower (upper) boundary of the full energy spectrum at positive (negative)  $\chi-\frac{1}{2}$ . The other boundary of the spectrum at  $L\to\infty$  is at zero energy. It corresponds to the state in which the total momentum p of the system is distributed among an infinite number of bosons with infinitesimal momentum.

We showed so far that at  $\chi=0$  and  $\chi\to\pm\infty$ , the eigenstates of the Hamiltonian (19) with a given momentum p are confined to regions with the boundaries that scale as  $p^3$ . Because both contributions to the Hamiltonian density in Eq. (19) have scaling dimension 4, this observation holds for any value of  $\chi$ . Furthermore, the form of the Hamiltonian (19) ensures that for any given  $\chi$  all the energies are proportional to  $\gamma$ . Thus the upper and lower boundaries of the spectrum can be presented in the form

$$\varepsilon_{\rm mKdV}(p) = \alpha_{\pm}(\chi)\gamma p^3.$$
 (24)

The above results for  $\chi=0$  and  $\chi\to\pm\infty$  can be summarized as

$$\alpha_{+}(\chi) = \begin{cases} \frac{1}{2} - \chi, & \chi \to -\infty, \\ 1, & \chi = 0, \\ 0, & \chi \to +\infty, \end{cases}$$
 (25)

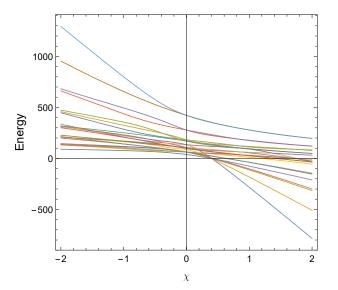


FIG. 3. The energy spectrum of the Hamiltonian (19) for the total momentum P=8 in units of  $2\pi\hbar/L$ . The units are chosen so that  $\gamma=\hbar=1$  and  $L=2\pi$ . The solid lines show the positions of the 22 energy levels for each value of the parameter  $\chi$ . (We have subtracted P/4=2 from all eigenvalues to account for the term  $-(\pi^2\hbar^2\gamma/L^2)\hat{P}$  in Eq. (18) [17].) At  $\chi=0$  the two highest energy states are degenerate, corresponding to the single quasiparticle and quasihole with energies  $\left(P-\frac{1}{2}\right)^3+\frac{1}{8}=422$ .

and

$$\alpha_{-}(\chi) = \begin{cases} 0, & \chi \to -\infty, \\ 0, & \chi = 0, \\ \frac{1}{2} - \chi, & \chi \to +\infty. \end{cases}$$
 (26)

The Hamiltonian (19) can be diagonalized numerically for moderate values of the total momentum p. The results for the full energy spectrum in the case of  $p=8\times 2\pi\hbar/L$  are shown in Fig. 3. The functions  $\alpha_+(\chi)$  and  $\alpha_-(\chi)$  can then be computed by extrapolating the energies of the highest and lowest levels to the limit  $L\to\infty$  at fixed p, see Fig. 4.

The function  $\alpha_-(\chi)$  shows two distinct types of behavior. When the dimensionless interaction parameter is large and positive  $(\chi \to +\infty)$ ,  $\alpha_-$  scales as  $\frac{1}{2}-\chi$ , in agreement with Eq. (26). As we discussed, the corresponding lowest energy state of the system at a given value p of the total momentum has a single bosonic excitation with momentum p. As  $\chi$  is lowered,  $\alpha_-(\chi)$  increases until it reaches zero at  $\chi = \chi_c \approx 0.4$ . At  $\chi < \chi_c$  the lowest possible energy of the system remains zero. As we saw earlier, this is indeed the case for  $\chi = 0$  and  $\chi \to -\infty$ , see Eq. (26). The lowest energy state in these cases corresponded to the total momentum p being distributed among an infinite number of elementary excitations with infinitesimal momentum. The numerical results of Fig. 4 imply that this is the case for all  $\chi < \chi_c$ .

The behavior of the function  $\alpha_{+}(\chi)$ , which describes

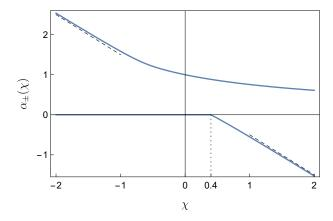


FIG. 4. The functions  $\alpha_+(\chi)$  and  $\alpha_-(\chi)$  evaluated numerically [17] are shown by the top and bottom solid lines, respectively. The dashed lines represent the result  $\frac{1}{2} - \chi$  for the bosonic excitation branch, Eq. (23), which controls one of the boundaries at large  $|\chi|$ , see Eqs. (25) and (26). Note that at  $\chi < \chi_c \approx 0.4$  we have  $\alpha_-(\chi) = 0$ .

the upper boundary of the spectrum, is qualitatively different. It scales as  $\frac{1}{2}-\chi$  at large negative  $\chi,$  which corresponds to the energy of the system with a single bosonic excitation, see Eqs. (23) and (25). It decreases gradually as  $\chi$  increases. At  $\chi=0$  it reaches the value  $\alpha(0)=1,$  corresponding to a state of free chiral Fermi gas with a single quasiparticle or quasihole excitation. It continues to decrease at positive  $\chi$  and gradually approaches zero at  $\chi\to+\infty,$  see Eq. (25). The nature of the highest energy state at  $\chi\gg 1$  is not self-evident, but our discussion in Sec. II suggests that it may be related to the classical soliton solutions of the modified KdV equation.

#### C. Solitons

To study the classical limit of the Hamiltonian (19), we use the commutation relation (11) to write the equation of motion for the operator  $\phi(x,t)$ ,

$$\frac{1}{\hbar^2 \gamma} \partial_t \phi = -(\partial_x \phi)^3 + \left(\frac{1}{2} - \chi\right) \partial_x^3 \phi. \tag{27}$$

In the classical limit,  $\phi(x,t)$  is no longer an operator, and thus we ignored normal ordering. The conditions under which this approximation is applicable will be established later.

Next, we introduce  $\tau = \hbar^2 \gamma t$ , differentiate Eq. (27) with respect to x, and obtain a partial differential equation for the function

$$u(x,\tau) = \partial_x \phi(x,\tau) \tag{28}$$

in the form

$$\partial_{\tau}u + 3u^2 \partial_x u + \tilde{\chi} \partial_x^3 u = 0, \quad \tilde{\chi} = \chi - \frac{1}{2}.$$
 (29)

This is the well-known classical modified KdV equation [18]. At  $\tilde{\chi}>0$  it has two soliton solutions

$$u(x,\tau) = \pm \frac{\sqrt{2c}}{\cosh\left(\sqrt{\frac{c}{\tilde{\chi}}}(x - c\tau)\right)},$$
 (30)

where c > 0. No soliton solutions exist for  $\tilde{\chi} < 0$ .

We are now in a position to obtain the condition of applicability of the classical approximation used in deriving Eq. (27). Equation (30) yields the order of magnitude estimate  $u \sim \sqrt{c}$ . Given that the spatial scale of the soliton solution is  $\sqrt{\tilde{\chi}/c}$ , Eq. (28) yields  $\phi \sim u\sqrt{\tilde{\chi}/c} \sim \sqrt{\tilde{\chi}}$ . According to Eq. (11), the commutator of  $\phi(x)$  and  $\phi(y)$  is of order unity. Classical approximation assumes that it is small compared to  $\phi(x)\phi(y) \sim \tilde{\chi}$ . Thus the classical results are applicable at  $|\tilde{\chi}| \gg 1$  or, equivalently,  $|\chi| \gg 1$ .

Integrating the standard bosonization expression for the particle density  $n(x) = \partial_x \phi/2\pi = u/2\pi$  with respect to x, we find the total number of fermions carried by a single soliton

$$N_s = \pm \sqrt{\frac{\tilde{\chi}}{2}}. (31)$$

Thus, at  $\tilde{\chi} \gg 1$ , when the classical mKdV theory applies to the chiral Fermi system with cubic dispersion, the soliton carries a large number of particles,  $|N_s| \gg 1$ .

Next, we substitute Eq. (28) into Eq. (7) and (19) to obtain the expressions for the momentum and energy of the soliton (30) in the limit  $L \to \infty$ . This yields

$$p = \frac{\hbar}{4\pi} \int_{-\infty}^{\infty} u^2 dx = \frac{\hbar}{\pi} \sqrt{c\tilde{\chi}},$$

$$E = \frac{\hbar^3 \gamma}{8\pi} \int_{-\infty}^{\infty} \left( u^4 + (1 - 2\chi) u'^2 \right) dx = \frac{\hbar^3 \gamma}{3\pi} \sqrt{c^3 \tilde{\chi}}.$$

These expressions give the dispersion relation for the soliton in the form

$$E(p) = \frac{\pi^2}{3\tilde{\chi}} \gamma p^3. \tag{32}$$

As expected, the energy scales with the third power of momentum.

Similarly to the case of a system of chiral fermions with quadratic dispersion discussed in Sec. II, soliton behaves as an elementary excitation of the system. Although states involving many solitons are possible, the convex shape of the dispersion relation (32) suggests that the state with one soliton has the largest energy at a given momentum. This implies the following behavior of  $\alpha_+(\chi)$  at large  $\chi$ ,

$$\alpha_{+}(\chi) \simeq \frac{2\pi^{2}}{3(2\chi - 1)}, \quad \chi \gg 1,$$
 (33)

where we used Eqs. (24), (32), and the definition of  $\tilde{\chi}$  from Eq. (29). The asymptotic behavior (33) is consistent with our earlier expectation of the limiting value at

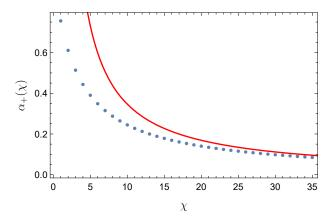


FIG. 5. Comparison of the numerically computed  $\alpha_{+}(\chi)$  for  $\chi = 1, 2, ..., 35$  (dots) with the asymptotic behavior (33) shown by the solid line.

 $\chi \to +\infty$  in Eq. (25). It can also be compared with the numerical results for  $\alpha_+(\chi)$ , but this requires extending the computation to much larger values of  $\chi$  than those shown in Fig. 4. Such a comparison shows a good agreement at  $\chi \gtrsim 20$ , see Fig. 5.

### D. Interpretation in terms of elementary excitations

In Sec. II we discussed the dispersions (12) of the elementary excitations of the quantum KdV model (8) and demonstrated that they also define the boundaries of the many-body spectrum of the system at  $L \to \infty$ . The elementary excitations were studied in Ref. [9] with the help of the Bethe ansatz solutions of the Lieb-Liniger [14] and hyperbolic Calogero-Sutherland [16] models, which reduce to the quantum KdV model under proper limiting procedures. Unfortunately, no mapping of this kind is known for the quantum mKdV model (19). Furthermore, even though this model is believed to be integrable [10], a Bethe ansatz solution is not currently available. Thus, we so far focused on obtaining the boundaries of the manybody spectrum of the Hamiltonian (19) at  $L \to \infty$ . We now discuss to what extent they can be interpreted as elementary excitations of the system.

We start with the case of noninteracting fermions. If the dispersion is quadratic, the quasiparticle and quasihole with momentum p have energies  $p^2/2m$  and  $-p^2/2m$ , respectively. These values are the highest and the lowest possible energies of any eigenstate with the total momentum p. In contrast, if the dispersion is cubic, both the quasiparticle and quasihole have the same energy  $\gamma p^3$ , which can be interpreted as a consequence of the particle-hole symmetry of the Hamiltonian. Due to the convexity of the dispersion  $\gamma p^3$ , it also yields the upper boundary of the many-body spectrum. The lowest energy state can be constructed by distributing the total momentum p among a large number of quasiparticles and

quasiholes [17]. At  $L \to \infty$ , the corresponding energy is 0.

A similar interpretation of the boundaries of the spectrum applies in the limit of strong attractive interactions,  $\chi \to -\infty$ . In this case, to leading order the Hamiltonian takes the form (23). The highest energy state has a single bosonic excitation,

$$\psi_o(p) = b_p^{\dagger} |0\rangle, \quad E_o(p) = \gamma \left(\frac{1}{2} - \chi\right) p^3.$$
 (34)

Here the subscript 'o' indicates that the state contains an odd number of bosonic excitations, which means that it is odd with respect to the particle-hole symmetry, see Eq. (21). The highest energy even state is

$$\psi_e(p) = b_{p-p_1}^{\dagger} b_{p_1}^{\dagger} |0\rangle, \quad E_e(p) \simeq E_o(p) \left(1 - \frac{3p_1}{p}\right), \quad (35)$$

where  $p_1 = 2\pi\hbar/L$ . In the limit of infinite system size, the respective energies are equal,  $E_o(p) = E_e(p)$ . The lowest energy eigenstates of the Hamiltonian (23) with large negative  $\chi$  in the two parity sectors are

$$(b_{p_1}^{\dagger})^{\frac{p}{p_1}}|0\rangle, \quad (b_{p_1}^{\dagger})^{\frac{p}{p_1}-2}b_{2p_1}^{\dagger}|0\rangle.$$
 (36)

The corresponding energies vanish at  $L \to \infty$ .

In the above examples the system has two branches of elementary excitations, which correspond to states that are even and odd with respect to particle-hole symmetry, with energies that become identical at  $L \to \infty$ . The dispersion  $\varepsilon(p)$  of the excitations defines the upper boundary of the excitation spectrum of the quantum mKdV Hamiltonian (19), while the lower boundary is at zero energy. Our results for the boundaries of the energy spectrum at  $L \to \infty$  given by Eq. (24) and Fig. 4 suggest that the same picture applies at all  $\chi < \chi_c \approx 0.4$ . Then the dispersion of the elementary excitations is

$$\varepsilon_{\text{mKdV}}^+(p) = \alpha_+(\chi)\gamma p^3.$$
 (37)

The function  $\alpha_+(\chi)$  shown by the upper line in Fig. 4 continues into the region  $\chi > \chi_c$ , suggesting that the excitation branch with dispersion given by Eq. (37) exists at all interaction strengths. On the other hand, the lower boundary of the spectrum corresponds to negative energies at  $\chi > \chi_c$ . Furthermore, at  $\chi \to \infty$  the approximation (23) applies again. The dispersion associated with the two excitation branches (34) and (35) is now concave and thus describes the lower boundary of the energy spectrum. This suggests that in addition to the excitation branch (37), there is another one, with dispersion

$$\varepsilon_{\mathrm{mKdV}}^{-}(p) = \alpha_{-}(\chi)\gamma p^{3}, \quad \chi > \chi_{c}.$$
 (38)

Our results for the boundaries of the spectrum do not preclude the possibility that this branch continues into the region  $\chi < \chi_c$ . Indeed, a mode with energy  $\alpha^* \gamma p^3$ 

would not affect the boundaries of the many-body spectrum at  $\chi < \chi_c$  as long as  $0 < \alpha^* < \alpha_+$ . We note, however, that at  $\chi = 0$ , when the model describes free fermions, quasiparticles and quasiholes are the only types of excitations present, and their dispersion is given by Eq. (37). Thus the branch (38) must terminate at some value of  $\chi$  between 0 and  $\chi_c$ . Some numerical evidence supporting this scenario is obtained by studying overlaps of the single boson state with all the eigenstates of the Hamiltonian with  $0 < \chi < \chi_c$  [17].

#### IV. DISCUSSION OF THE RESULTS

In Sec. II we studied the elementary excitations and the boundaries of the many-body spectrum of the system of spinless chiral fermions with short-range interactions. Upon bosonization the problem reduces to the quantum KdV model (8), for which exact results for the excitation spectrum are available [9]. We concluded that at  $p \ll p^*$ the excitations are essentially the quasihole and quasiparticle of the free Fermi gas, while at  $p \gg p^*$ , they are the bosonic density wave and the KdV soliton. Taking into consideration the definition (13) of  $p^*$ , this can be alternatively interpreted as crossover between the regimes of weak and strong interactions. Given the curvature of the dispersions of the two excitation branches, Fig. 1, it is natural to expect that they would coincide with the lowest and highest energies of many-body states with total momentum p. This conjecture is confirmed by our numerical calculations.

Our main focus was on the study of the system of interacting spinless chiral fermions with cubic dispersion, Sec. III. Bosonization reduces this problem to the quantum mKdV model (19). The scaling properties of this model dictate that the energy scales associated with it must be proportional to  $p^3$ . This applies, in particular, to the boundaries of the many-body spectrum, which we obtained numerically, see Eq. (24) and Fig. 4. Unlike the case of quadratic dispersion studied in Sec. II, we found two distinct regimes of interaction strength. At  $\chi > \chi_c$ the system behaves similarly to the quantum KdV model (8) in that both boundaries of the many-body spectrum can be viewed as states with one elementary excitation. The excitation belongs to one of two branches, with dispersions given by Eqs. (37) and (38). This analogy fails at  $\chi < \chi_c$ , where only the upper boundary of the excitation spectrum behaves as an elementary excitation; its dispersion is given by Eq. (37). At  $\chi = 0$  and  $\chi \to -\infty$ the lower boundary corresponds to states with infinite number of excitations, each carrying infinitesimal momentum. It is natural to apply the same interpretation to the lower boundary of the spectrum at all  $\chi < \chi_c$ .

The existence of two qualitatively different regimes depending on the interaction strength could have been anticipated by considering the limit of strong interactions,  $|\chi| \to \infty$ . In this limit the system is described by the classical mKdV equation (29). The latter has harmonic

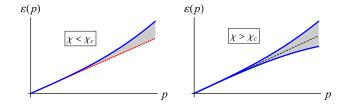


FIG. 6. Boundaries of the many-body spectrum of the system of chiral fermions with cubic dispersion and short-range interactions. For all  $\chi$  the upper boundary is given by  $\varepsilon = vp + \varepsilon_{\mathrm{mKdV}}^+(p)$ , see Eq. (37). At  $\chi < \chi_c$  the lower boundary of the spectrum is the straight dotted line  $\varepsilon = vp$ , while at  $\chi > \chi_c$  it is given by  $\varepsilon = vp + \varepsilon_{\mathrm{mKdV}}^-(p)$ , see Eq. (38).

wave solutions with infinitesimal amplitude, for which the nonlinear term in Eq. (29) can be neglected. They correspond to the bosonic excitations giving the upper (lower) boundary of the spectrum at  $\chi \to -\infty$  ( $\chi \to +\infty$ ). In addition, at  $\tilde{\chi} > 0$  the mKdV equation (29) has soliton solutions. In analogy with the quantum KdV model (8), the soliton gives the upper boundary of the excitation spectrum, see Sec. III C. In contrast, no solitons solutions exist at  $\tilde{\chi} < 0$ , resulting in the qualitatively different behavior of the lower boundary of the spectrum at  $\chi \to -\infty$ .

The energy eigenvalues of the original model of chiral fermions with cubic dispersion are related to those of the quantum mKdV model by Eq. (22). Our results are illustrated in Fig. 6, where the boundaries of the energy spectrum are shown in the two regimes,  $\chi < \chi_c$  and  $\chi > \chi_c$ . The behavior of the energy spectrum in the latter regime is similar to that for fermions with quadratic dispersion, see Fig. 1.

Let us now briefly discuss the expected behavior of the dynamic response functions of the system, which include the spectral function  $A(p,\epsilon)$  and the dynamic structure factor  $S(p,\epsilon)$ . The shaded regions in Figs. 1 and 6 correspond to the possible energies of the system at a given momentum. The response functions must vanish outside these regions. In nonchiral systems the behavior of  $A(p,\epsilon)$  and  $S(p,\epsilon)$  near the edge of support was studied phenomenologically using the mobile impurity model [19, 20]. This approach should be applicable near the boundaries of the spectrum of chiral fermions with quadratic dispersion, which allow for the interpretation as states with one elementary excitation. It should also apply to the boundaries shown by solid lines in Fig. 6 for the case of fermions with cubic dispersion. In the nonchiral case both  $A(p,\epsilon)$  and  $S(p,\epsilon)$  were predicted to scale as a power of the distance from the boundary [19, 20]. We expect an analogous power-law scaling in the chiral

The lower boundary of the spectrum at  $\chi < \chi_c$ , shown by the dotted line in Fig. 6, has a different nature. The states near this boundary involve a large number of excitations with very small momenta. A similar problem has been studied in the case of phonons in liquid helium, where the exponential suppression of the response was found [21]. In the case of one-dimensional systems with linear spectrum, equivalent to the limit  $\chi \to -\infty$  of our model, the exponential suppression of the spectral function was found in Ref. [22]. Furthermore, in the case of weakly interacting fermions,  $|\chi| \ll 1$ , the overlap of a low-energy state involving a large number of particle-hole pairs with that involving a single pair occurs in a high order of the perturbation theory. As a result, the response functions must again be exponentially small near the boundary. We therefore expect exponential suppression of the dynamic response functions near the lower boundary of the spectrum at  $\chi < \chi_c$ . Our numerical treatment of the Hamiltonian (19) supports this conclusion [17].

The qualitative change of the energy spectrum at the interaction strength  $\chi=\chi_c$  can be interpreted as a phase transition in the system. Interestingly, this phase transition is purely dynamic, in that it appears only in the dynamic response functions of the system. Indeed, due to the chiral nature of the problem, the ground state  $|0\rangle$ , which corresponds to the filled Fermi surface, does not depend on the interaction strength. Thus the static prop-

erties of the system are not affected by the interactions. Alternatively, one can consider the behavior of the system at a fixed value p of the total momentum. In this case the ground state energy as a function of the interaction strength  $\chi$  shows nonanalytic behavior at  $\chi=\chi_c$ , which can be interpreted as a quantum phase transition. A similar nonanalytic behavior of the boundary of the energy spectrum at a fixed momentum was recently found in the system of chiral fermions with quadratic spectrum and Coulomb interactions [23]. Finally, we note that in our numerical data represented in Fig. 4 we have not been able to find a deviation of  $\chi_c$  from 0.4, i.e., we expect that the exact value is  $\chi_c = \frac{2}{5}$ .

#### ACKNOWLEDGMENTS

The author is grateful to A. Furusaki, I. Martin, M. R. Norman, and M. Pustilnik for helpful discussions. This work was supported by the U.S. Department of Energy, Office of Science, Basic Energy Sciences, Materials Sciences and Engineering Division.

- E. M. Lifshitz and L. P. Pitaevskii, Statistical Physics, Part 2 (Butterworth-Heinemann, Oxford, 1980).
- [2] F. D. M. Haldane, 'Luttinger liquid theory' of onedimensional quantum fluids. I. Properties of the Luttinger model and their extension to the general 1D interacting spinless Fermi gas, J. Phys. C: Solid State Phys. 14, 2585 (1981).
- [3] T. Giamarchi, Quantum physics in one dimension (Clarendon, Oxford, 2004).
- [4] C. L. Kane and M. P. A. Fisher, Transmission through barriers and resonant tunneling in an interacting onedimensional electron gas, Phys. Rev. B 46, 15233 (1992).
- [5] A. Furusaki and N. Nagaosa, Single-barrier problem and Anderson localization in a one-dimensional interacting electron system, Phys. Rev. B 47, 4631 (1993).
- [6] J. M. Luttinger, An Exactly Soluble Model of a Many-Fermion System, J. Math. Phys. 4, 1154 (1963).
- [7] A. V. Rozhkov, Fermionic quasiparticle representation of Tomonaga-Luttinger Hamiltonian, Eur. Phys. J. B 47, 193 (2005).
- [8] M. Pustilnik and K. A. Matveev, Solitons in a onedimensional Wigner crystal, Phys. Rev. B 91, 165416 (2015).
- [9] M. Pustilnik and K. A. Matveev, Fate of classical solitons in one-dimensional quantum systems, Phys. Rev. B 92, 195146 (2015).
- [10] R. Sasaki and I. Yamanaka, Field theoretical construction of an infinite set of quantum commuting operators related with soliton equations, Comm. Math. Phys. 108, 691 (1987).
- [11] A. K. Pogrebkov, Boson-fermion correspondence and quantum integrable and dispersionless models, Russ. Math. Surv. 58, 1003 (2003).

- [12] B. I. Halperin, Quantized Hall conductance, currentcarrying edge states, and the existence of extended states in a two-dimensional disordered potential, Phys. Rev. B 25, 2185 (1982).
- [13] For an interaction potential that falls off as a power of the distance x between the fermions,  $U(x) \propto 1/|x|^{\lambda}$  at  $|x| \to \infty$ , this condition requires  $\lambda > 3$ .
- [14] E. H. Lieb and W. Liniger, Exact Analysis of an Interacting Bose Gas. I. The General Solution and the Ground State, Phys. Rev. 130, 1605 (1963).
- [15] B. Sutherland, A brief history of the quantum soliton with new results on the quantization of the Toda lattice, Rocky Mount. J. of Math. 8, 413 (1978).
- [16] B. Sutherland, Beautiful Models: 70 Years of Exactly Solved Quantum Many-body Problems (World Scientific, Singapore, 2004).
- [17] For details, see Supplemental Material.
- [18] G. L. Lamb, Elements of soliton theory (Wiley, New York, 1980).
- [19] A. Imambekov and L. I. Glazman, Phenomenology of One-Dimensional Quantum Liquids Beyond the Low-Energy Limit, Phys. Rev. Lett. 102, 126405 (2009).
- [20] A. Imambekov, T. L. Schmidt, and L. I. Glazman, Onedimensional quantum liquids: Beyond the Luttinger liquid paradigm, Rev. Mod. Phys. 84, 1253 (2012).
- [21] S. V. Iordanskii and L. P. Pitaevskii, Properties of the endpoint of a multiphonon spectrum, JETP Lett. 27, 621 (1978).
- [22] K. A. Matveev, Spectral Function of the Chiral One-Dimensional Fermi Liquid in the Regime of Strong Interactions, Phys. Rev. Lett. 128, 176802 (2022).
- [23] I. Martin and K. A. Matveev, Scar states in a system of interacting chiral fermions, Phys. Rev. B 105, 045119 (2022).

# Elementary excitations of a system of one-dimensional chiral fermions with short-range interactions

-Supplemental Material-

K. A. Matveev

Materials Science Division, Argonne National Laboratory, Argonne, Illinois 60439, USA

## S1. NUMERICAL TREATMENT OF THE QUANTUM KDV HAMILTONIAN (8)

We start by setting N=0 and choosing the units in which  $\hbar=m=1$  and  $L=2\pi$ . We then use the expression (5) for  $\phi(x)$  to rewrite the Hamiltonian (8) in terms of the bosonic operators  $b_l$  and  $b_l^{\dagger}$ ,

$$H_{\text{KdV}} = \frac{1}{2} \sum_{l=2}^{\infty} \sum_{l'=1}^{l-1} \sqrt{ll'(l-l')} \left( b_l^{\dagger} b_{l'} b_{l-l'} + b_{l'}^{\dagger} b_{l-l'}^{\dagger} b_l \right) - \frac{\eta}{2\pi} \sum_{l=1}^{\infty} l^3 b_l^{\dagger} b_l.$$
 (S1)

We now fix the total momentum P of the system and construct the basis of the Hilbert space by partitioning momentum as a sum  $P = \sum_l ln_l$  over all bosonic states l with occupation numbers  $n_l$ . Each integer partition of P defines a unique basis state. In this basis the Hamiltonian (S1) is a real symmetric matrix. The dimension of the Hilbert space is number of integer partitions of P. We perform subsequent calculations for P up to 48, for which there are 147273 integer partitions.

Next, we find the highest and the lowest eigenstates of the Hamiltonian,  $E_+$  and  $E_-$ , numerically for several values of the interaction constant  $\eta$ . It is convenient to present the results in terms of the parameter  $s = p/p^* = pm\eta/\pi\hbar$ , which in our units becomes  $s = \eta P/\pi$ . In Fig. S1 we plot  $E_{\pm}(s)$  normalized by  $E_+(0) = P(P-1)/2$ , which ensures that the ratio is  $\pm 1$  at s = 0.

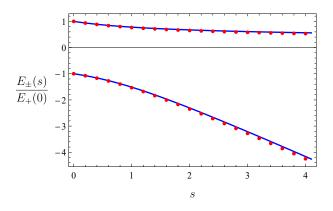


FIG. S1. Comparison of the quasiparticle energies (12) with the spectral boundaries of the Hamiltonian (8). The solid lines are  $e_{\pm}(s)/s^2$ , cf. Fig. 2. The dots represent the numerically computed boundaries of the energy spectrum  $E_{\pm}(s)$  of the Hamiltonian (8) for P=48, rescaled by  $E_{+}(0)$ .

Numerical results for  $E_{\pm}(s)/E_{+}(0)$  are compared with  $e_{\pm}(s)/s^{2}$ , which is the expected result for the system of infinite size, see Sec. II. In our calculation the dimensionless momentum is  $P = pL/2\pi\hbar$ . Thus the limit  $L \to \infty$  at fixed p corresponds to  $P \to \infty$ . The data for P = 48, see Fig. S1, shows good, but not perfect agreement, especially at larger values of s.

Since the dimension of the Hilbert space grows exponentially with P, we cannot increase P indefinitely. On the other hand, our data can be reliably extrapolated to  $P \to \infty$ . To illustrate the procedure we show in Fig. S2 the computed values of  $E_{\pm}(4)/E_{+}(0)$  (bottom right red dot in Fig. S1) for even values of P between 4 and 48. We then fit the data points for P=42, 44, 46, and 48 to the function

$$f(P) = A_0 + \frac{A_1}{P} + \frac{A_2}{P^2} + \frac{A_3}{P^3}$$
 (S2)

and find the coefficients  $A_0$ ,  $A_1$ ,  $A_2$ , and  $A_3$ . The resulting function f(P) is shown by the solid line in Fig. S2. Given the excellent quality of the fit, we conclude that replacing the computed value of  $E_{\pm}(4)/E_{+}(0)$  for P=48 with  $f(\infty)=A_0$  will accurately extrapolate the results to infinite system size. We perform this fitting procedure for all the points shown in Fig. S1. The resulting data is shown in Fig. 2.

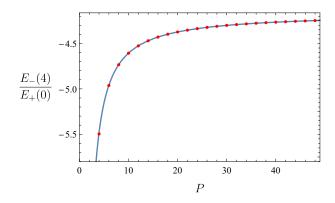


FIG. S2. The ratio  $E_{-}(4)/E_{+}(0)$  evaluated for the even values of the total momentum P from 4 to 48. Solid line is the fit of the form (S2) using four data points P = 42, 44, 46, and 48.

#### S2. NUMERICAL TREATMENT OF THE QUANTUM MKDV HAMILTONIAN (19)

We again set N=0 and choose the units so that  $\hbar=\gamma=1$  and  $L=2\pi$ . Substitution of Eq. (5) into the Hamiltonian (19) yields

$$H_{\text{mKdV}} = \sum_{l=1}^{\infty} \sum_{l'=1}^{\infty} \sum_{l''=1}^{\infty} \sqrt{ll'l''(l+l'+l'')} \left( b_l^{\dagger} b_{l'}^{\dagger} b_{l''}^{\dagger} b_{l+l'+l''} + b_{l+l'+l''}^{\dagger} b_l b_{l'} b_{l''} \right)$$

$$+ \frac{3}{2} \sum_{l=2}^{\infty} \sum_{l'=1}^{l-1} \sum_{l''=1}^{l-1} \sqrt{l'(l-l')l''(l-l'')} b_{l'}^{\dagger} b_{l-l'}^{\dagger} b_{l''} b_{l-l''} + \left( \frac{1}{2} - \chi \right) \sum_{l=1}^{\infty} l^3 b_l^{\dagger} b_l.$$
(S3)

To study the energy spectrum of this Hamiltonian at a fixed value of the total momentum P, we use the approach described in Sec. S1, see the comments below Eq. (S1).

#### A. Eigenvalues

In Fig. 3 we show all 22 eigenvalues of the Hamiltonian  $H_{\rm mKdV}-\frac{1}{4}\hat{P}$  for P=8 and the interaction strength parameter in the range  $-2\leq\chi\leq 2$ . Compared to the operator  $H_{\rm mKdV}$ , for which the relevant energy scales are proportional to  $P^3$ , the term  $-\hat{P}/4$  is small and amounts to a finite-size correction. The origin of this term is the contribution  $-(\pi^2\hbar^2\gamma/L^2)\hat{P}$  in Eq. (18). In the case of zero interaction,  $\chi=0$ , the operator  $H_{\rm mKdV}-\frac{1}{4}\hat{P}$  is the exact bosonized form of the operator

$$H_3 = \sum_{p} \left( p - \frac{1}{2} \right)^3 a_p^{\dagger} a_p, \tag{S4}$$

where the momentum p in our units takes integer values; cf. Eqs. (1) and (17). At a given total momentum P the maximum eigenvalues of  $H_3$  correspond to a single fermion moved from the highest occupied state p=0 to the state with p=P (quasiparticle), or from p=1-P to p=1 (quasihole). In both cases the energy is

$$E_3^{\text{max}}(P) = \left(P - \frac{1}{2}\right)^3 + \frac{1}{2^3}$$
 (S5)

In the case of P=8 we have  $E_3^{\rm max}(8)=422$  which agrees with the maximum eigenvalue at  $\chi=0$  in Fig. 3. The full set of the 22 numerically obtained eigenvalues of  $H_{\rm mKdV}-\frac{1}{4}\hat{P}$  at  $\chi=0$  is

$$E=422.,422.,278.,278.,182.,182.,170.,170.,134.,134.,\\107.,107.,98.,98.,86.,62.,62.,62.,62.,62.,62.,62.,38.$$

It is easy to check directly that they are exactly the eigenvalues of the Hamiltonian (S4) at total momentum P = 8.

#### **B.** Evaluation of $\alpha_{\pm}(\chi)$

To obtain the results for  $\alpha_+(\chi)$  shown by the top line in Fig. 4, we obtain the highest eigenvalue of the Hamiltonian  $H_{\text{mKdV}} - \frac{1}{4}\hat{P}$  with a given  $\chi$  for P between 10 and 40. We then fit the data for the four highest values of P to a cubic polynomial

$$B_0 + B_1 P + B_2 P^2 + B_3 P^3$$

and identify  $\alpha_+(\chi)$  as the coefficient  $B_3$ . (Since in physical units  $P = pL/2\pi\hbar$ , extrapolation to  $P \to \infty$  is equivalent to taking the limit  $L \to \infty$  at fixed physical momentum p.) The fits are excellent, see Fig. S3; the results for  $\alpha_+(\chi)$  are shown by the upper line in Fig. 4. The same method is used to obtain the results for  $\alpha_-(\chi)$  shown by the lower line in Fig. 4 at  $\chi > 0.4$ .

The fitting procedure described above cannot be applied to the evaluation of  $\alpha_{-}(\chi)$  at  $\chi < 0.4$ . To illustrate the difficulty, we consider the case  $\chi = 0$ , which corresponds to the free fermion Hamiltonian (S4). If  $P = n^2$ , where n is integer, the eigenstate with the lowest energy is obtained from  $|0\rangle$  by moving fermions from n highest

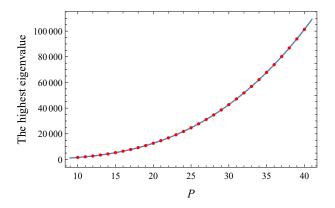


FIG. S3. The dots represent the numerically obtained results for the highest eigenvalue of the Hamiltonian  $H_{\rm mKdV}-\frac{1}{4}\hat{P}$  for  $\chi=-1$  and  $P=10,11,\ldots,40$ . The solid line is the cubic polynomial  $1.5849P^3-0.019308P^2-2.5392P+12.884$  obtained by fitting the the data for P=37,38,39, and 40. The fit yields  $\alpha_+(-1)\approx 1.585,$  cf. Fig. 4.

occupied states to n lowest empty states,

$$a_n^{\dagger} \dots a_2^{\dagger} a_1^{\dagger} a_0 a_{-1} \dots a_{-(n-1)} |0\rangle.$$

The corresponding energy is  $(2n^4-n^2)/4 = (2p^2-p)/4$ . If

 $n^2 , the total number of displaced fermions remains <math>n$ . The extra momentum  $p-n^2$  is accommodated by moving some of the newly created particles above the Fermi level up in momentum by 1 and/or some of the new holes down by 1. The resulting lowest eigenvalue is

$$E_3^{\min}(P) = \begin{cases} \frac{1}{4} \left( 2P^2 - P \right), & P = n^2, \\ \frac{1}{8} \left( 4n^4 + 8n^3 + 10n^2 + 6n + 1 - \left( 2n^2 + 2n + 1 - 2P \right)^3 \right), & n^2 < P \le n^2 + n, \\ \frac{1}{8} \left( 4n^4 + 16n^3 + 22n^2 + 12n + 1 - \left( 2n^2 + 4n + 1 - 2P \right)^3 \right), & n^2 + n < P \le n^2 + 2n, \end{cases}$$
(S6)

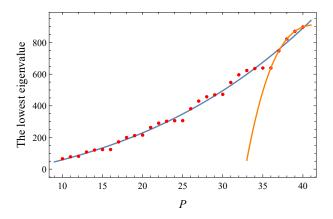


FIG. S4. The lowest eigenvalue  $E_3^{\min}(P)$  of the Hamiltonian (S4) for the total momentum  $P = 10, 11, \ldots, 40$ . The blue line is the best fit of the data to a cubic polynomial. The orange line is the same fit using only the last four data points.

where n is the integer part of  $\sqrt{P}$ . It is easy to see that  $E_3^{\min}(P)$  grows as  $P^2/2$  at  $P \to \infty$ . This yields

$$\alpha_{-}(0) = \lim_{P \to \infty} \frac{E_3^{\min}(P)}{P^3} = 0.$$

We show  $E_3^{\min}(P)$  for P between 10 and 40 in Fig. S4. Clearly, fitting the last four data points (P=37, 38, 39, 40) yields a wrong trend at large P. On the other hand, a fit using all the data points in Fig. S4, yields  $0.00547362P^3 + 0.151921P^2 + 8.64975P - 48.2719$ , corresponding to  $\alpha_-(0) = 0.00547362 \ll 1$ . This small value of  $\alpha_-(0)$  is a reasonable approximation to the exact analytical result  $\alpha_-(0) = 0$ .

We apply this fitting procedure to the lowest energy eigenvalues for all  $\chi < 0.4$  and find  $|\alpha_{-}(\chi)| \leq \alpha_{-}(0)$  in the whole range  $-2 < \chi < 0.4$ . We thus conclude that to the numerical accuracy,  $\alpha_{-}(\chi) = 0$  for all  $\chi < \chi_c \approx 0.4$ , as shown in Fig. 4.

#### C. Overlap of some eigenstates

In Sec. IV we argued that the behavior of the dynamic response functions at the lower boundary of the spectrum is qualitatively different in the regimes  $\chi < \chi_c$  and  $\chi > \chi_c$ . Specifically, both the spectral function and the dynamic structure factor are expected to show power-law dependence on the distance from the lower boundary at  $\chi > \chi_c$  and be exponentially suppressed at  $\chi < \chi_c$ . Here, we consider the dynamic structure factor, which in bosonic variables is given by

$$S_p(\epsilon) = p \sum_j |\langle j | b_P^{\dagger} | 0 \rangle|^2 \delta(\epsilon - E_j), \tag{S7}$$

where  $p = (2\pi\hbar/L)P$ , the summation is over all the eigenstates  $|j\rangle$  of the Hamiltonian (S3), and the  $E_j$  is the energy of the state  $|j\rangle$  measured from that of the vacuum state  $|0\rangle$ .

The exact diagonalization of the Hamiltonian (S3) yields both the eigenstates and the overlaps  $\langle j|b_P^{\dagger}|0\rangle$ . However, numerical evaluation of  $S_n(\epsilon)$  in the limit  $L \to \infty$  $\infty$  using Eq. (S7) is not straightforward, as the dimension of the Hilbert space grows exponentially with P. Our argument is Sec. IV was that at  $\chi < \chi_c$  the states near the lower boundary of the spectrum involve a large number of quasiparticles, which should result in an exponentially small overlap with the state  $b_P^{\dagger}|0\rangle$ . This can be demonstrated numerically. In Fig. S5 we show the dependence of  $|\langle 1|b_{P}^{\dagger}|0\rangle|^2$  on P, where  $|1\rangle$  is the lowest energy eigenstate of the Hamiltonian (S3). For  $\chi = 0.39$ , which is slightly below the crossover value  $\chi_c \approx 0.4$ , the overlap drops sharply with increasing P. A closer examination of the data shows an exponential dependence of the overlap on P. At P=40 we obtained  $|\langle 1|b_P^{\dagger}|0\rangle|^2\approx 4\times 10^{-30}$ . A similar behavior is observed for other values of  $\chi$  below  $\chi_c$ . On the other hand, for  $\chi > \chi_c$  the overlap shows only a weak dependence on P.

At the end of Sec. III [below Eq. (38)] we mentioned the possibility of the second branch of elementary excitations existing at  $0 < \chi < \chi_c$ . The energy of this mode  $\alpha^* \gamma p^3$  would have to be positive but lower than the energy of the first branch (37), i.e.,  $0 < \alpha^* < \alpha_+$ . To

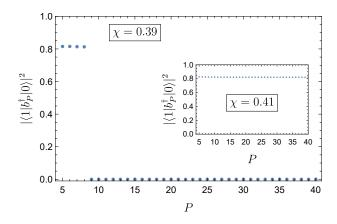


FIG. S5. Dependence of  $|\langle 1|b_P^{\dagger}|0\rangle|^2$  on P for  $\chi=0.39<\chi_c$  and P from 5 to 40. At  $P\geq 9$  the overlap is very small. In contrast, at  $\chi=0.41>\chi_c$  (inset) the overlap is close to 0.8 for all P.

explore this possibility, we evaluated the overlaps of the single boson state  $b_P^{\dagger}|0\rangle$  with all the eigenstates  $|j\rangle$  of the Hamiltonian (S3) for various values of P and  $\chi$ . For a given  $\chi$ , we then identified the state with the largest overlap  $|\langle j|b_P^{\dagger}|0\rangle|^2$  for each P and obtained the corresponding energy  $E^*(P)$ . After numerical extrapolation to  $P\to\infty$ , we obtained  $\alpha^*=\lim_{P\to\infty}E^*(P)/P^3$ . The dependence  $\alpha^*(\chi)$  is shown in Fig. S6.

We note that at  $\chi < 0$  the state with the largest overlap with  $b_P^{\dagger}|0\rangle$  is the highest energy state. Thus,

$$\alpha^*(\chi) = \alpha_+(\chi), \quad \chi < 0. \tag{S8}$$

In other words, at negative  $\gamma$  our procedure has identified

the previously obtained branch of elementary excitations (37). On the other hand, at  $\chi > \chi_c \approx 0.4$  the maximum overlap is achieved for the ground state of the system, i.e.,

$$\alpha^*(\chi) = \alpha_-(\chi), \quad \chi > \chi_c. \tag{S9}$$

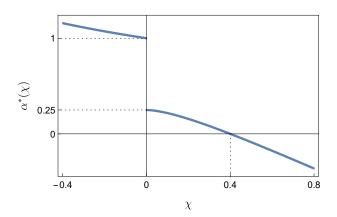


FIG. S6. Function  $\alpha^*(\chi)$  that parametrizes the energy  $\alpha^*P^3$  of the eigenstate  $|j\rangle$  that has the largest overlap with the single boson state  $b_p^{\dagger}|0\rangle$ .

In this case our procedure yields the lower of the two branches of elementary excitations, Eq. (38). In the limits  $\chi \to \pm \infty$  the results (S8) and (S9) were expected, because in the interaction-dominated regimes bosons are elementary excitations of the system.

The data shown in Fig. S6 suggests that the lower branch (38) of the elementary excitations at  $\chi > \chi_c$  continues into the region  $0 < \chi < \chi_c$ , where its energy is positive. The latter property, corresponding to  $\alpha^* > 0$  in Fig. S6, means that this branch is no longer associated with the ground state of the system.